Tuning the redox activity of encapsulated metal clusters via the metallic and semiconducting character of carbon nanotubes

Fan Zhang[a], Xiulian Pan[a,1], Yongfeng Hu[b], Liang Yu[a], Xiaoqi Chen[a], Peng Jiang[a], Hongbo Zhang[a], Shibin Deng[c], Jin Zhang[c], Trudy B. Bolin[d], Shuo Zhang[e], Yuying Huang[e], and Xinhe Bao[a,1]

[a]State Key Laboratory of Catalysis, Dalian Institute of Chemical Physics, Chinese Academy of Sciences, Dalian 116023, China; [b]Canadian Light Source Inc., Saskatoon, SK, Canada S7N 2V3; [c]College of Chemistry and Molecular Engineering, Peking University, Beijing 100871, China; [d]Advanced Photon Source, Argonne National Laboratory, Argonne, IL 60439; and [e]Shanghai Synchrotron Radiation Facility, Shanghai Institute of Applied Physics, Chinese Academy of Sciences, Shanghai 201204, China

Edited by Alexis T. Bell, University of California, Berkeley, CA, and approved July 29, 2013 (received for review April 12, 2013)

We demonstrate that reactions confined within single-walled carbon nanotube (SWCNT) channels are modulated by the metallic and semiconducting character of the hosts. In situ Raman and X-ray absorption near-edge structure spectroscopies provide complementary information about the electronic state of carbon nanotubes and the encapsulated rhenium species, which reveal electronic interactions between encapsulated species and nanotubes. More electrons are transferred from metallic tubes (m-SWCNTs) to oxidic rhenium clusters, leading to a lower valence state rhenium oxide than that in semiconducting tubes (s-SWCNTs). Reduction in 3.5% (vol/vol) H_2/Ar leads to weakened host–guest electronic interaction. The high valence state Re within s-SWCNTs is more readily reduced when raising the temperature, whereas only a sluggish change is observed for Re within m-SWCNTs. Only at 400 °C does Re reach a similar electronic state (mixture of Re^0 and Re^{4+}) in both types of tubes. Subsequent oxidation in 1% O_2/Ar does not show changes for Re in s-SWCNTs up to 200 °C. In comparison, m-SWCNTs facilitate the oxidation of reduced rhenium (160 °C). This can be exploited for rational design of active catalysts with stable species as a desired valence state can be obtained by selecting specific-type SWCNTs and a controlled thermal treatment. These results also provide a chemical approach to modulate reversibly the electronic structure of SWCNTs without damaging the sidewalls of SWCNTs.

confined catalysis | confinement effect

An increasing number of studies reveal that confinement of metal or metal oxide nanoparticles inside carbon nanotubes (CNTs) often leads to significantly enhanced catalytic activity with respect to the same bare metal nanoparticles or those deposited on the outer walls of CNTs (1–3). Such a different behavior originates from both the physical (spatial restriction of the channels) and chemical factors (electronic interaction of confined species with the curved graphene walls) inside CNTs (1–5). In this sense, single-walled carbon nanotubes (SWCNTs) are very interesting because they have a higher degree of uniformity and smaller channel compared with multiwalled CNTs (6). More interestingly, they exhibit intrinsically either metallic or semiconducting properties with different electronic structure around the Fermi level. Metallic and semiconducting SWCNTs (m-SWCNTs and s-SWCNTs, respectively) have been demonstrated to vary significantly in reactivity toward covalent and noncovalent functionalization of their sidewalls (7–9). For example, diazonium salts (10), nitronium ions (NO_2^+) (11), and OsO_4 (12) reacted selectively with metallic tubes, which was attributed to their higher electron density near the Fermi level. Metallic tubes were also reported preferentially etched away by water and methane plasma because of their higher reactivity (13, 14). On the other hand, H_2O_2 (15), azomethineylides (16), and gaseous SO_3 (17) preferentially attacked s-SWCNTs, and recently s-SWCNTs were also shown to be preferentially polycarboxylated via reductive sidewall functionalization (18). However, it has not been studied yet if confinement of metal cluster catalysts within metallic and semiconducting SWCNTs affects chemical reactions differently. This understanding is essential for applications not only in catalysis but also nanoelectronics and sensoring.

Therefore, we investigated the encapsulation, redox properties, and catalytic behavior of metal species within the channels of metallic and semiconducting SWCNTs, respectively. Rhenium was chosen as a probe because it is of great technological importance in heterogeneous catalysis, e.g., olefin metathesis (19, 20), selective oxidation (21), and hydrodesulfurization (22). It was recently reported that the encapsulated metallic Re clusters and rhenium carbide deriving from rhenium carbonyl and fullerene can interact directly with the CNT interior surface activated by electron beam (5, 23, 24). However, it remains to be elucidated if the catalytic activity of rhenium cluster can be tuned by the intrinsic electronic state of the nanotube itself. Thus, simple model reactions such as reduction in hydrogen and oxidation in oxygen were studied to demonstrate the modulation effects of the SWCNT electronic structures, i.e., metallic vs. semiconducting characters. By monitoring the electronic state of rhenium and SWCNTs with in situ X-ray absorption near-edge structure (XANES) and in situ Raman spectroscopy, respectively, it is revealed that the redox activities of such encapsulates

Significance

The unique property of carbon nanotube channels has triggered wide research interest in different fields. An increasing number of studies show that confinement of metal or metal oxide nanoparticles inside these channels often leads to significantly modified catalytic activity with respect to the same bare metal nanoparticles or those dispersed on the outer walls. We demonstrate here that reactions can be further modulated by the electronic nature (metallic vs. semiconducting character) of nanotubes by taking encapsulated rhenium nanocatalysts as a probe. Particularly, the chemical state of the encapsulated rhenium is tuned due to host–guest electronic interaction. This is of significance for catalytic reactions sensitive to the chemical state of active metals, because it may change the reaction pathways.

Author contributions: X.P. and X.B. designed research; F.Z., X.P., Y. Hu, L.Y., X.C., P.J., H.Z., and S.D. performed research; J.Z., T.B.B., S.Z., and Y. Huang contributed new reagents/analytic tools; F.Z., X.P., Y. Hu, L.Y., X.C., and X.B. analyzed data; and F.Z., X.P., and X.B. wrote the paper.

The authors declare no conflict of interest.

This article is a PNAS Direct Submission.

[1]To whom correspondence may be addressed. E-mail: panxl@dicp.ac.cn or xhbao@dicp.ac.cn.

This article contains supporting information online at www.pnas.org/lookup/suppl/doi:10.1073/pnas.1306784110/-/DCSupplemental.

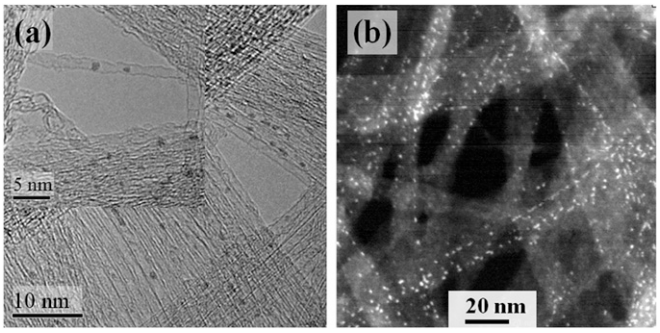

Fig. 1. (*A*) TEM image of metallic SWCNTs encapsulated with Re species. (*Inset*) One isolated tube is highlighted. (*B*) HAADF-STEM image of Re@m-SWCNTs. (Scale bar: 20 nm.)

are distinctly different within metallic and semiconducting tubes under the same reaction conditions.

Results

Prepurified m-SWCNTs and s-SWCNTs were purchased from NanoIntegris Inc. in the form of thin films composed of randomly tangled tubes. Both SWCNT samples exhibit a radial breathing mode (RBM) in a narrow and similar region of 150–170 cm^{-1} in the resonance Raman spectra. These RBM modes can be translated to a diameter of 1.4–1.6 nm according to an equation: $\omega_{(RBM)} = (234/d + 10)$, where $\omega_{(RBM)}$ represents the frequency of RBM mode (cm^{-1}) and d the diameter of the nanotube (nm) (25). SEM shows that the overall morphology of the SWCNTs remains intact upon encapsulation with rhenium species. A high-resolution transmission electron microscope (TEM) image in Fig. 1*A* shows that m-SWCNTs contain discrete particles of around 1 nm within the channels with the inset displaying such an individual tube. The high-angle annular dark-field scanning transmission electron microscopy (HAADF-STEM) image (Fig. 1*B*) indicates homogeneous dispersion of the encapsulated metal particles. TEM does not detect obvious differences in the morphology between fresh Re@s-SWCNTs (Fig. S1) and Re@m-SWCNTs. Scanning across the specimen, most rhenium species are observed within the channels (over 90%). Analysis of different regions of the specimen with energy-dispersive X-ray (EDX) (Fig. S2) indicates that Re is homogeneously distributed in both samples, and the two samples have a comparable Re loading (Re@s-SWCNTs 5.5 wt% and Re@m-SWCNTs 6.0 wt%).

XANES is an element-specific technique involving the excitation of electrons from a core level to the local and partial empty states of a defined absorption atom and is sensitive to its chemical state. Therefore, we used in situ XANES to monitor the chemical state of rhenium encapsulated in both m- and s-SWCNTs during reduction and oxidation processes. The Re L_3-edge XANES spectra in Fig. 2 show that the rhenium species in the fresh Re@s-SWCNTs have a valence state between +6 and +7 by comparison with the reference materials Re metal foil, ReO_2 and ReO_3 (Fig. S3) (26). In contrast, the absorption edge of rhenium within m-SWCNTs is about 1.0 ± 0.5 eV lower than those within s-SWCNTs and the chemical state is close to +4. It implies that the oxidic rhenium species within m-SWCNTs have accepted more electrons than those in s-SWCNTs. Note that the filling has been carried out in the same reactor with two parallel channels packed with m- and s-SWCNTs, respectively. The same precursor, filling procedure, and filling conditions have been applied. Because the two types of SWCNTs have a similar diameter and a similar Re loading, the different chemical state of rhenium species is likely related with the different electronic structures of s- and m-SWCNTs.

Therefore, we turn to Raman spectroscopy for examination of the electronic state of SWCNTs. CNTs are known to give a characteristic G band in the resonance Raman spectrum, which is associated with sp^2 hybridization and is sensitive to perturbation of the electronic structure (25). The G band of SWCNTs is usually split into two components, G^+ and G^-. The G^+ feature is associated with vibrations along the nanotube axis. Its frequency ω_{G+} is sensitive to charge transfer. For example, a blue shift of the G^+ band was observed in the Br_2-doped SWCNTs (27) and graphite intercalation compounds, due to the electron withdrawal from SWCNTs to acceptors leading to a contraction and hardening of the sp^2 lattice. The G^- feature is related with vibrations along the circumference. It generally exhibits a narrow Lorentzian line shape for semiconducting tubes, whereas there is a long tail at the lower energy side for metallic ones, known as a Breit–Wigner–Fano (BWF) line originating from coupling of the discrete phonons to an electronic continuum. Charge transfer also leads to an intensity increase or decrease of the BWF feature (28). These distinct features have been frequently used to distinguish s- and m-SWCNTs, and to examine their electronic structures (29).

For this purpose, we have grown isolated SWCNTs on a marked SiO_2/Si substrate, which makes it convenient to identify individual tubes. Fig. 3 shows SEM and atomic force microscope (AFM) images as well as Raman spectra of m- and s-SWCNTs with and without encapsulated Re species. Fig. 3*A* shows an individual tube located close to the marks. AFM indicates a height of 1.8 ± 0.2 nm for this tube (Fig. 3*B*). At an excitation energy of 1.96 eV, an RBM mode around 146.5 cm^{-1} is observed (Fig. 3*C*), which corresponds to a diameter of 1.7 nm. This is consistent with the AFM measurement, confirming that this is a single nanotube instead of a bundle. The G^+ band exhibits a narrow Lorentzian line shape at 1,590 cm^{-1} with a narrow and weaker G^- band at 1,570 cm^{-1} (Fig. 3*D*), characteristic for a semiconducting tube. Therefore, the tube is denoted as s-SWCNT. Upon encapsulation with rhenium species (Re@s-SWCNT), the G mode of the same tube reduces drastically in its intensity (normalized by the Si phonon mode in Fig. 3*C*). Fig. 3*D* shows the enlarged G region. One sees that it is blue-shifted by 7 cm^{-1} compared with the blank s-SWCNT. Fig. 3*E* shows another individual nanotube with the height measured to be 1.6 ± 0.2 nm by AFM (Fig. 3*F*). The Raman RBM signal at 160.8 cm^{-1} (Fig. 3*G*) indicates a diameter of 1.6 nm. This nanotube gives a G band with a BWF line (Fig. 3*H*), characteristics for a metallic tube (m-SWCNT). Upon encapsulation, the intensity of the G mode and particularly the BWF line decreases even more prominently with respect to the pristine tube. The G^+ band is blue-shifted by 18 cm^{-1} (Fig. 3*H*). Furthermore, statistical analysis of eight semiconducting tubes and three metallic tubes on SiO_2/Si substrates shows that the G^+ mode shifts in a range of 12–18 cm^{-1} for Re@m-SWCNT in contrast with 4–7 cm^{-1} for Re@s-SWCNT.

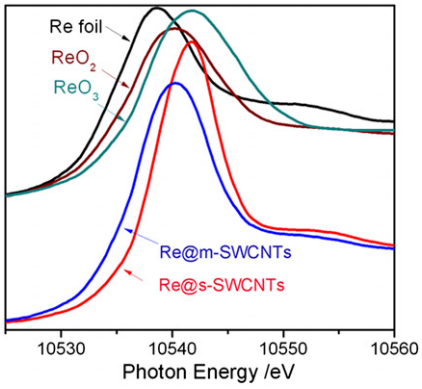

Fig. 2. Re L_3-edge XANES spectra of fresh Re@s-SWCNT and Re@m-SWCNT along with reference materials of Re foil, ReO_2, and ReO_3.

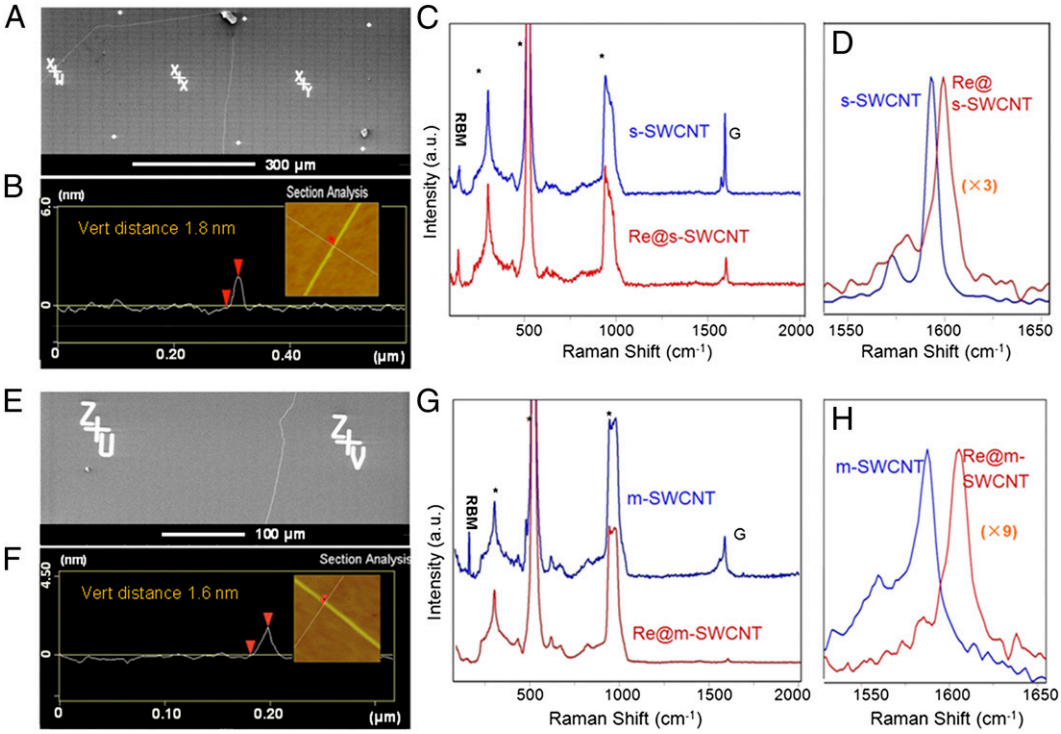

Fig. 3. (*A*) SEM and (*B*) AFM image, (*C* and *D*) Raman spectra of an individual s-SWCNT (blue spectrum) before and after encapsulation with Re species (Re@s-SWCNT, red spectrum); (*E*) SEM and (*F*) AFM image, (*G* and *H*) Raman spectra of an individual m-SWCNT (blue spectrum) before and after encapsulation (Re@m-SWCNT, red spectrum). The spectra in (*C*) and (*G*) are normalized with Si mode, and the bands marked with "*" corresponds to Si modes. (*D*) and (*H*) are enlarged G modes in different magnitudes for comparison.

Examination of the s-SWCNTs and m-SWCNTs film samples also indicates a blue shift of the G^+ mode by ~8 cm^{-1} for metallic tubes in contrast with ~4 cm^{-1} for semiconducting ones upon encapsulation with rhenium species. However, the G^- mode is split into several components and the G^+ and G^- modes are less defined for the film sample than the individual tube because the former contains usually bundles of SWCNTs with a certain distribution of diameters.

The strain effects induced by the curvatures, which may also cause a blue shift of the G^+ band, can be neglected here because the two types of SWCNTs have a similar diameter and a similar Re loading. Cronin et al. reported a reduced intensity for the BWF line and a blue-shifted G^+ band when an SWCNT interacted with dilute H_2SO_4 solution upon a large positive voltage due to depletion of free electrons on the SWCNT surface (30). Tsang et al. also observed a blue-shifted and narrowed G mode when a large external gate field was applied on an SWCNT (29). Therefore, the changes of the G band (Fig. 3) can be attributed to electron transfer from the nanotubes to the encapsulated oxidic rhenium species, and this transfer is more prominent within metallic nanotubes. It is likely due to a higher electron density at the Fermi level (10) and a smaller ionization potential (31) of m-SWCNTs than their semiconducting counterparts. This has been proposed to be responsible for the higher reactivity of m-SWCNTs than s-SWCNTs with some electrophilic compounds (32), such as diazonium salts (10) and OsO_4 (12). Consequently, rhenium should exhibit a lower valence state within m-SWCNTs than those in s-SWCNTs, as we have observed in XANES. In addition, the RBM bands down-shift slightly, their intensity changes, and in some cases the RBM band almost disappears upon encapsulation. Similar changes have also been observed previously for the RBM modes due to charge transfer between the encapsulated species and the nanotube (25, 33).

The above results indicate that the encapsulated rhenium species interact differently with semiconducting and metallic tubes. We further studied the chemical reactivity of the confined clusters in simple reduction and oxidation processes, and their relation with the electronic structure of CNTs. Fig. 4*A* shows that rhenium species within s-SWCNTs remain stable and the chemical state starts to change only above 200 °C upon reduction in 3.5% H_2/Ar, as evidenced by the slightly down-shifted Re L_3 absorption edge. Partial reduction of Re_2O_7 within unsorted SWCNTs by pure H_2 stream was also reported previously (34). Above 300 °C, a significant reduction of Re is observed within s-SWCNTs. At 400 °C part of Re is reduced to Re^0, as evidenced by the first derivative of the spectrum (Fig. 4*A*, *Inset*). Incomplete reduction of rhenium even at 450 °C in hydrogen was also reported for Re/Al_2O_3 (35, 36). Interestingly, rhenium species within m-SWCNTs are even more stable. As shown in Fig. 4*B*, the Re absorption edge does not change obviously up to 300 °C. There is only a slightly increasing fraction of metallic rhenium whereas the oxide almost remains Re^{+4}. After reduction at 400 °C, the spectrum for Re@m-SWCNTs almost overlaps with that of Re@s-SWCNTs. It indicates that rhenium species within the two types of nanotubes reach a similar final chemical state (a mixture of Re^0 and Re^{4+}).

In situ Raman spectra (Fig. 5) show that the G^+ band of both Re@s-SWCNTs and Re@m-SWCNTs red-shifts stepwise with the rising temperature and at the same time the G^- band is broadened during reduction in 3.5% H_2/Ar. Note that blank s-SWCNTs and m-SWCNTs subjected to the same treatment in hydrogen do not show any observable change. It indicates that electron transfer from m- and s-SWCNTs to the encapsulated Re species is more and more attenuated with increasing reduction of the Re clusters (filling of empty Re d states). Fig. 5*A* and 5*C* shows that the G^+ band of Re@s-SWCNTs starts to shift at 200 °C in hydrogen. With the temperature increasing up to 300 °C, it is close

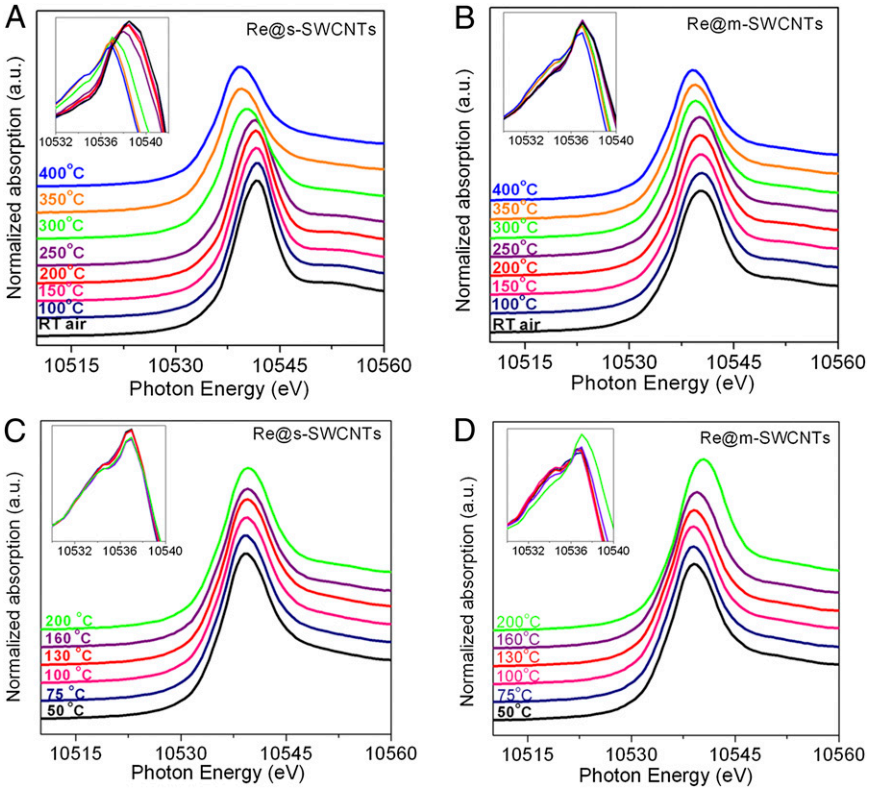

Fig. 4. In situ Re L3 XANES spectra for (*A*) Re@s-SWCNTs and (*B*) Re@m-SWCNTs during reduction in 3.5% H_2/Ar; (*C*) Re@s-SWCNTs and (*D*) Re@m-SWCNTs during oxidation in 1% O_2/Ar at different temperatures. (*Insets*) First derivatives of the corresponding XANES spectra.

to that of the pristine s-SWCNTs and the shape of the G^- band also resembles the pristine tubes (Fig. 5*A*). This indicates that the electronic structure of the nanotubes is restored with respect to the pristine s-SWCNTs at this temperature. In comparison, the G^+ band of Re@m-SWCNTs starts to shift at 250 °C and a higher temperature (over 350 °C) is needed for it to recover the electronic state of the pristine m-SWCNTs (Fig. 5*B* and 5*C*). This trend is consistent with the XANES results. After reduction at 400 °C, the G^- band further grows broader beyond the position of the pristine ones for both s-SWCNTs and m-SWCNTs, indicating that the nanotubes received electrons. Because the rhenium species within the two types of SWCNTs have reached a similar chemical state eventually as partially reduced Re^0 and Re^{4+}, we wondered whether the oxidation of these rhenium species would exhibit complementary behavior.

Although rhenium is highly oxophilic and apt to oxidation (37), the following oxidation experiments demonstrate that confinement within SWCNTs provides some protection against oxidation. For example, subsequent exposure of the reduced Re@s-SWCNTs (at 400 °C) to 1% O_2/Ar does not oxidize the encapsulated rhenium even at 200 °C. As evidenced by the unchanged Re L_3 edge in Fig. 4*C*, rhenium remains at the final state of the reduction

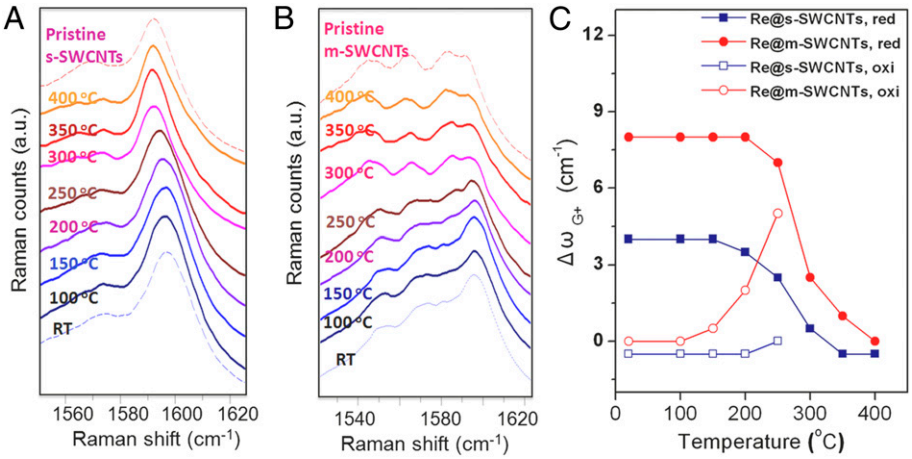

Fig. 5. In situ Raman spectra for the G band for (*A*) Re@s-SWCNTs and (*B*) Re@m-SWCNTs during reduction in 3.5% H_2/Ar. (*C*) G^+ band changes of Re@s-SWCNTs and Re@m-SWCNTs with respect to the pristine s-SWCNTs and m-SWCNTs as a function of reduction and oxidation temperatures. Spectra were recorded at room temperature to avoid the temperature effect.

process. In contrast, rhenium is much easier to oxidize within m-SWCNTs, because the absorption edge of Re L_3 starts to shift to a higher energy above 160 °C. After treatment at 200 °C, the valence state of Re is slightly above +4, similar to that in the fresh Re@m-SWCNTs (Fig. 4*D*). Suppressed oxidation was also observed previously for Fe nanoparticles confined within multiwalled carbon nanotubes (MWCNTs), compared with the particles dispersed on the outer walls of nanotubes, as evidenced by temperature-programmed oxidation monitored by an online mass spectrometer and microbalance, as well as in situ X-ray diffraction (XRD) (38). The results in this study reveal that the extent of suppression further depends on the electronic structure of nanotubes. s-SWCNTs provide a better protection for rhenium clusters against oxidation, whereas within m-SWCNTs the oxidation is relatively more facile. Previous studies showed that m-SWCNTs reacted more readily with O_2 than s-SWCNTs, due to the higher electron density near the Fermi level (39). Thus, the adsorbed oxygen molecules could help facilitate the oxidation of rhenium clusters within m-SWCNTs.

Correspondingly, the Raman G^+ band of the reduced Re@s-SWCNTs does not change much further even when the sample is heated up to 200 °C in oxygen (Figs. S4*A* and 5*C*). In comparison, exposure of the reduced Re@m-SWCNTs to oxygen above 150 °C leads to a gradual shift of the G^+ toward that of the fresh Re@m-SWCNTs. At the same time, the G^- region (BWF shape) becomes narrower and the intensity reduces (Fig. S4*B*). It suggests that m-SWCNTs donate electrons to rhenium upon oxidation above 150 °C whereas s-SWCNTs do not below 200 °C, as shown by in situ XANES and Raman spectrosopy. These results also show that the band structure of SWCNTs can be selectively tuned with encapsulated rhenium species and a controlled redox process. Furthermore, the intensity ratio of the G/D bands normalized to the pristine nanotubes, which has been frequently used as an indicator of the disordered degree in sp^2 hybridized carbon, does not change obviously following reduction and oxidation, and no morphology change is observed. It implies that the main framework of SWCNTs remains almost intact, which is important for other applications such as electronic devices and sensors. In addition, the changes of G modes of Re@s-SWCNTs and Re@m-SWCNTs are observed to be reversible in reduction and oxidation cycles. Therefore, encapsulation also provides a chemical approach to modulate the electronic structure of SWCNTs without damaging the sidewalls of SWCNTs.

The above in situ Raman and XANES spectroscopic results provide complementary information about the electronic state of CNTs and rhenium during reduction and oxidation. It clearly reveals interaction between encapsulated species and nanotubes. This lends further support to the concept that electron transfer from/to the curved graphene walls of CNTs could play an important role in the catalytic activity of confined catalysts, as it has been observed previously (2, 40). For example, reduction of iron oxide (38, 41) and ruthenium oxide (42) was facilitated, whereas oxidation of metallic iron was retarded within MWCNTs due to interaction between the confined materials and the CNT surfaces (38). The improved reducibility of the confined iron catalyst favored formation of iron carbide species under Fischer–Tropsch synthesis conditions, which consequently led to a significantly higher activity (41, 43). We expect that the modulated reduction and oxidation activities of the encapsulated rhenium can also be used to tune a series of catalytic reactions (44).

In conclusion, studies with in situ Raman spectroscopy and in situ XANES demonstrate that the reduction and oxidation activities of the encapsulated rhenium species can be modulated by utilization of metallic or semiconducting SWCNT tubes. This is attributed to the different host–guest interaction dictated by the electronic structure of SWCNTs. As a result, the metallic tubes donate more electrons to the confined rhenium oxide species leading to a lower valence state of rhenium with respect to the semiconducting tubes. Reduction in hydrogen leads to weakened electron transfer between rhenium and nanotubes. The high valence state Re within s-SWCNTs is more readily reduced. The encapsulated rhenium reaches a similar state in m- and s-SWCNTs upon reduction at 400 °C. The reduced rhenium is protected within SWCNTs from oxidation in 1% O_2/Ar. No oxidation is observed up to 200 °C within s-SWCNTs, whereas it is more facile within m-SWCNTs. Correspondingly, m-SWCNTs donate electrons again as rhenium is oxidized. Therefore, by selecting a specific type of SWCNTs and thermal treatment conditions one may obtain a stabilized rhenium species with different valence states. This is of significance for numerous catalytic reactions, which are sensitive to the chemical state of active metals. These results also point to a unique chemical approach for reversible modulation of the electronic structure of SWCNTs leaving the sidewalls of SWCNTs intact for applications in other fields such as electronic devices and sensors.

Materials and Methods

Catalyst Preparation. m-SWCNTs and s-SWCNTs were purchased from Nano-Integris Inc. (IsoNanotubes 90% and 99%). They had been produced by the electric arc discharge process followed by separation with a density-gradient ultracentrifugation method. The samples contain trace impurities, as indicated by neutron activation analysis from the provider (www.nanointegris.com/en/downloads). Ends were opened during purification. The intensity ratio of Raman D/G bands for both pristine s-SWCNT and m-SWCNT samples is around 0.049–0.053, indicating very few defects. Volatile methyltrioxorhenium [$Re(CH_3)O_3$] was used as the precursor for encapsulation. Filling has been carried out in the same reactor with two parallel channels packed with m- and s-SWCNTs, respectively, to make sure that the same precursor, filling procedure, and filling conditions have been applied for each set of m- and s-SWCNTs. Six sets of m-SWCNTs and s-SWCNTs have been repeatedly prepared and each set has a comparable Re loading. The reactor was evacuated to 10^{-4} Pa at 420 °C before exposing SWCNTs to $Re(CH_3)O_3$. The mixture was kept at 90 °C for 48 h. Subsequently, the sample was treated with dilute HNO_3 (0.1 M) or excess ethanol at room temperature to remove rhenium species on the outer walls and washed with deionized water thoroughly until the filtrate reached pH value of ~7. Blank s-SWCNTs and m-SWCNTs were subjected to the same HNO_3 washing, and Raman spectroscopy indicates that both G and D bands remained almost unchanged after washing. The resulting encapsulates within m-SWCNTs and s-SWCNTs are denoted Re@m-SWCNTs and Re@s-SWCNTs, respectively. For comparison, individual SWCNTs were also grown on Si/SiO_2 wafers using an established chemical vapor deposition method (45). The as-synthesized SWCNTs were heated in air at 400 °C for 30 min to remove amorphous carbon and to open caps. The same procedure and conditions as those for the film samples were applied to introduce rhenium species into these individual tubes.

Catalyst Characterization. The morphology and composition of the catalysts were characterized with scanning electron microscope (SEM) equipped with an EDX analyzer (FEI Quanta 200F, operated at 1 kV), atomic force microscope (AFM, Veeco multimode 3D), and high-resolution transmission electron microscope [HRTEM, Tecnai F30 field emission gun (FEG)-TEM at 300 kV].

In Situ Reduction and Oxidation. In situ Raman spectroscopy was undertaken on a LabRAM HR 800 Raman spectrometer using the 1.96-eV laser as the exciting source. For individual SWCNT, the maximum intensity was 3 mW and no damage of the sample was observed. For SWCNT film sample, the maximum intensity was ~0.5 mW. The sample was pressed onto a thin Si wafer and mounted in the in situ cell (Linkam CCR1000 stage). It was heated up from 100 °C to 400 °C in a flow of 3.5% (vol/vol) H_2/Ar and was treated at selected temperatures for 30 min before cooling down in a flow of pure Ar. Spectra were recorded at room temperature to avoid the temperature effect. Subsequently, the in situ cell was purged with Ar. Then, a mixture of 1% O_2/Ar was fed into the in situ cell. The oxidation was also allowed for 30 min at each temperature up to 250 °C and the spectra were recorded at room temperature. In situ XANES spectra were carried out at Beamline 9-BM-B of the Advanced Photon Source and the results were reproduced at the BL14W1 beamline of the Shanghai Synchrotron Radiation Facility. All Re L_3-edge XANES spectra were taken at a step of 0.5 eV through the edge region with the transmission mode. Energy calibration was performed with a Ta foil. The same reduction and oxidation conditions as those in Raman spectroscopy were followed, as shown in Fig. S5.

ACKNOWLEDGMENTS. The authors acknowledge the kind assistance from Dr. Jeffrey T. Miller during in situ XANES experiments at Argonne National Laboratory, Dr. Linyan Hu during AFM measurements at Dalian Institute of Chemical Physics, and Dr. Ting Yu for kind help on discussion of Raman spectra. This work was supported by Natural Science Foundation of China Grants 11079005, 21033009, and 21173215 and Ministry of Science and Technology Grant 2011CBA00503.

1. Serp P, Castillejos E (2010) Catalysis in carbon nanotubes. *ChemCatChem* 2(1): 41–47.
2. Pan X, Bao X (2011) The effects of confinement inside carbon nanotubes on catalysis. *Acc Chem Res* 44(8):553–562.
3. Centi G, Perathoner S (2011) Creating and mastering nano-objects to design advanced catalytic materials. *Coord Chem Rev* 255(13–14):1480–1498.
4. Kondratyuk P, Yates JT, Jr. (2007) Molecular views of physical adsorption inside and outside of single-wall carbon nanotubes. *Acc Chem Res* 40(10):995–1004.
5. Zoberbier T, et al. (2012) Interactions and reactions of transition metal clusters with the interior of single-walled carbon nanotubes imaged at the atomic scale. *J Am Chem Soc* 134(6):3073–3079.
6. Iijima S, Ichihashi T (1993) Single-shell carbon nanotubes of 1-nm diameter. *Nature* 363(6430):603–605.
7. Joselevich E (2004) Chemistry and electronics of carbon nanotubes go together. *Angew Chem Int Ed Engl* 43(23):2992–2994.
8. Kamaras K, Itkis ME, Hu H, Zhao B, Haddon RC (2003) Covalent bond formation to a carbon nanotube metal. *Science* 301(5639):1501.
9. Voggu R, Rao KV, George SJ, Rao CNR (2010) A simple method of separating metallic and semiconducting single-walled carbon nanotubes based on molecular charge transfer. *J Am Chem Soc* 132(16):5560–5561.
10. Strano MS, et al. (2003) Electronic structure control of single-walled carbon nanotube functionalization. *Science* 301(5639):1519–1522.
11. An KH, et al. (2005) A diameter-selective attack of metallic carbon nanotubes by nitronium ions. *J Am Chem Soc* 127(14):5196–5203.
12. Banerjee S, Wong SS (2004) Selective metallic tube reactivity in the solution-phase osmylation of single-walled carbon nanotubes. *J Am Chem Soc* 126(7):2073–2081.
13. Zhou W, Zhan S, Ding L, Liu J (2012) General rules for selective growth of enriched semiconducting single walled carbon nanotubes with water vapor as in situ etchant. *J Am Chem Soc* 134(34):14019–14026.
14. Zhou CW, Kong J, Yenilmez E, Dai HJ (2000) Modulated chemical doping of individual carbon nanotubes. *Science* 290(5496):1552–1555.
15. Miyata Y, Maniwa Y, Kataura H (2006) Selective oxidation of semiconducting single-wall carbon nanotubes by hydrogen peroxide. *J Phys Chem B* 110(1):25–29.
16. Ménard-Moyon C, Izard N, Doris E, Mioskowski C (2006) Separation of semiconducting from metallic carbon nanotubes by selective functionalization with azomethine ylides. *J Am Chem Soc* 128(20):6552–6553.
17. Zhang H, et al. (2009) A facile, low-cost, and scalable method of selective etching of semiconducting single-walled carbon nanotubes by a gas reaction. *Adv Mater* 21(7): 813–816.
18. Gebhardt B, et al. (2011) Selective polycarboxylation of semiconducting single-walled carbon nanotubes by reductive sidewall functionalization. *J Am Chem Soc* 133(48): 19459–19473.
19. Mol JC (1999) Olefin metathesis over supported rhenium oxide catalysts. *Catal Today* 51(2):289–299.
20. Moses AW, et al. (2007) Spectroscopically distinct sites present in methyltrioxorhenium grafted onto silica-alumina, and their abilities to initiate olefin metathesis. *J Am Chem Soc* 129(28):8912–8920.
21. Zhang H, et al. (2013) Enhancing chemical reactions in a confined hydrophobic environment: An NMR study of benzene hydroxylation in carbon nanotubes. *Chem Sci* 4(3):1075–1078.
22. Pecoraro TA, Chianelli RR (1981) Hydrodesulfurization catalysis by transition metal sulfides. *J Catal* 67(2):430–445.
23. Chamberlain TW, et al. (2011) Reactions of the inner surface of carbon nanotubes and nanoprotrusion processes imaged at the atomic scale. *Nat Chem* 3(9):732–737.
24. Chamberlain TW, et al. (2012) Formation of uncapped nanometre-sized metal particles by decomposition of metal carbonyls in carbon nanotubes. *Chem Sci* 3(6):1919–1924.
25. Dresselhaus MS, Dresselhaus G, Saito R, Jorio A (2005) Raman spectroscopy of carbon nanotubes. *Phys Rep* 409(2):47–99.
26. Ravel B, Scorzato C, Siddons DP, Kelly SD, Bare SR (2010) Simultaneous XAFS measurements of multiple samples. *J Synchrotron Radiat* 17(3):380–385.
27. Rao AM, Eklund PC, Bandow S, Thess A, Smalley RE (1997) Evidence for charge transfer in doped carbon nanotube bundles from Raman scattering. *Nature* 388(6639):257–259.
28. Corio P, et al. (2003) Potential dependent surface Raman spectroscopy of single wall carbon nanotube films on platinum electrodes. *Chem Phys Lett* 370(5-6):675–682.
29. Tsang JC, Freitag M, Perebeinos V, Liu J, Avouris P (2007) Doping and phonon renormalization in carbon nanotubes. *Nat Nanotechnol* 2(11):725–730.
30. Cronin SB, et al. (2004) Electrochemical gating of individual single-wall carbon nanotubes observed by electron transport measurements and resonant Raman spectroscopy. *Appl Phys Lett* 84(12):2052–2054.
31. Lu J, et al. (2006) Selective interaction of large or charge-transfer aromatic molecules with metallic single-wall carbon nanotubes: critical role of the molecular size and orientation. *J Am Chem Soc* 128(15):5114–5118.
32. Zhang H, Wu B, Hu W, Liu Y (2011) Separation and/or selective enrichment of single-walled carbon nanotubes based on their electronic properties. *Chem Soc Rev* 40(3): 1324–1336.
33. Débarre A, et al. (2003) Specific Raman signatures of a dimetallofullerene peapod. *Phys Rev Lett* 91(8):085501.
34. Costa PMFJ, Sloan J, Rutherford T, Green MLH (2005) Encapsulation of RexOy clusters within single-walled carbon nanotubes and their in tubulo reduction and sintering to Re metal. *Chem Mater* 17(26):6579–6582.
35. Fung AS, Tooley PA, Kelley MJ, Koningsberger DC, Gates BC (1991) Cationic trirhenium rafts on. gamma.-alumina: Characterization by x-ray absorption spectroscopy. *J Phys Chem* 95(1):225–234.
36. Rønning M, Nicholson D, Holmen A (2001) In situ EXAFS study of the bimetallic interaction in a rhenium-promoted alumina-supported cobalt Fischer–Tropsch catalyst. *Catal Lett* 72(3-4):141–146.
37. Bare SR, et al. (2011) Experimental (XAS, STEM, TPR, and XPS) and theoretical (DFT) characterization of supported rhenium catalysts. *J Phys Chem C* 115(13):5740–5755.
38. Chen W, Pan X, Bao X (2007) Tuning of redox properties of iron and iron oxides via encapsulation within carbon nanotubes. *J Am Chem Soc* 129(23):7421–7426.
39. Yu B, et al. (2010) Selective removal of metallic single-walled carbon nanotubes by combined in situ and post-synthesis oxidation. *Carbon* 48(10):2941–2947.
40. Khlobystov AN (2011) Carbon nanotubes: From nano test tube to nano-reactor. *ACS Nano* 5(12):9306–9312.
41. Abbaslou RMM, Tavassoli A, Soltan J, Dalai AK (2009) Iron catalysts supported on carbon nanotubes for Fischer–Tropsch synthesis: Effect of catalytic site position. *Appl Catal A Gen* 367(1–2):47–52.
42. Guo SJ, et al. (2010) Probing the electronic effect of carbon nanotubes in catalysis: NH (3) synthesis with Ru nanoparticles. *Chem-Eur J* 16(18):5379–5384.
43. Chen W, Fan Z, Pan X, Bao X (2008) Effect of confinement in carbon nanotubes on the activity of Fischer-Tropsch iron catalyst. *J Am Chem Soc* 130(29):9414–9419.
44. Lobo-Lapidus RJ, Gates BC (2009) Rhenium complexes and clusters supported on γ-Al2O3: Effects of rhenium oxidation state and rhenium cluster size on catalytic activity for n-butane hydrogenolysis. *J Catal* 268(1):89–99.
45. Kong J, Soh HT, Cassell AM, Quate CF, Dai HJ (1998) Synthesis of individual single-walled carbon nanotubes on patterned silicon wafers. *Nature* 395(6705):878–881.